JKAS
Journal of the Korean Astronomical Society
http://jkas.kas.org
eISSN: 2288-890X · pISSN: 1225-4614
JKAS (2024), **57**, 1, 95–103
doi: 10.5303/JKAS.2024.57.1.95

Eddington Ratios of Dust-Obscured Quasars at $z \sim 2$

Dohyeong Kim [1,2,⋆], Myungshin Im [3,4,⋆], Gu Lim [1,2], and Yongjung Kim [5]

[1]Department of Earth Sciences, Pusan National University, Busan 46241, Republic of Korea
[2]Institute for Future Earth (IFE), Pusan National University, Busan 46241, Republic of Korea
[3]Astronomy Program, Dept. of Physics & Astronomy, Seoul National University, Seoul 08826, Republic of Korea
[4]SNU Astronomy Research Center (SNU ARC), Astronomy Program, Dept. of Physics & Astronomy, Seoul National University, Seoul 08826, Republic of Korea
[5]Korea Astronomy and Space Science Institute, Daejeon 34055, Republic of Korea
⋆Corresponding Authors: D. Kim and M. Im, dh.dr2kim@gmail.com, myungshin.im@gmail.com

Received May 7, 2024; Accepted June 13, 2024; Published June 18, 2024

Abstract

In the merger-driven galaxy evolution scenario, dust-obscured quasars are considered to be an intermediate population between merger-driven star-forming galaxies and unobscured quasars; however, this scenario is still controversial. To verify this, it is necessary to investigate whether dust-obscured quasars have higher Eddington ratio ($\lambda_{\rm Edd}$) values than those of unobscured quasars, as expected in the merger-driven galaxy evolution scenario. In this study, we derive black hole (BH) masses of 10 dust-obscured quasars at $z \sim 2$, during the peak period of star-formation and BH growth in the Universe, using a newly derived mid-infrared (MIR) continuum luminosity ($L_{\rm MIR}$)-based estimator that is highly resistant to dust extinction. Then, we compare the $\lambda_{\rm Edd}$ values of these dust-obscured quasars to those of unobscured type-1 quasars at similar redshifts. We find that the measured $\log(\lambda_{\rm Edd})$ values of the dust-obscured quasars, -0.06 ± 0.10, are significantly higher than those of the unobscured quasars, -0.86 ± 0.01. This result remains consistent across the redshift range from 1.5 to 2.5. Our results show that the dust-obscured quasars are at their maximal growth, consistent with the expectation from the merger-driven galaxy evolution scenario at the epoch quasar activities were most prominent in the cosmic history.

Keywords: galaxies: evolution — galaxies: interactions — galaxies: quasars: emission lines — galaxies: quasars: general — galaxies: quasars: supermassive black holes

1. Introduction

To date, nearly a million quasars have been found through various surveys in X-ray, ultra violet (UV), optical, and radio wavelengths (e.g., Becker et al. 2001; Croom et al. 2004; Schneider et al. 2005; Véron-Cetty & Véron 2006). However, it has been reported that a significant number of dust-obscured quasars, which suffer from dust extinction caused by intervening dust in their host galaxies, can be missed (Comastri et al. 2001; Polletta et al. 2008) in soft X-ray, UV, and optical based quasar surveys. It is known that these dust-obscured quasars can account for up to ∼50% of the entire quasar population (e.g., Polletta et al. 2008). Recently, Kim et al. (2023) found that ∼15% of Sloan Digital Sky Survey (SDSS; York et al. 2000) quasars (Pâris et al. 2018), which were discovered based on optical surveys, are affected by dust extinction.

In a merger-driven galaxy evolution scenario, these dust-obscured quasars are expected as the intermediate population between merger-driven star-forming galaxies, often seen as ultra luminous infrared glaxies (ULIRGs; Sanders et al. 1988), and unobscured quasars. This merger-driven galaxy evolution scenario has been studied in several theoretical simulation studies (e.g., Menci et al. 2004; Hopkins et al. 2008), and several pieces of observational evidence support that dust-obscured quasars are the young quasars in the scenario. For example, dust-obscured quasars have (i) dusty red colors (Kim & Im 2018); (ii) high $\lambda_{\rm Edd}$ values (Urrutia et al. 2012; Kim et al. 2015a, 2018, 2024a); (iii) merging features in their host galaxies (Urrutia et al. 2008; Glikman et al. 2015); and (iv) merging SMBH system candidates (Kim et al. 2020), as expected in the simulation studies.

However, some previous studies have claimed that dust-obscured quasars are not the young quasars in the scenario. These studies suggested that the red colors of dust-obscured quasars could arise from (i) a moderate viewing angle in the unification model (Wilkes et al. 2002; Rose et al. 2013); or (ii) a unique intrinsic spectral energy distribution (SED) without dust extinction (Puchnarewicz & Mason 1998; Whiting et al. 2001). Moreover, the host galaxies of dust-obscured

quasars are the intermediate-age galaxies between young and old populations (Georgantopoulos et al. 2023), contrary to the merger-driven galaxy evolution scenario.

A key way to verify if dust-obscured quasars represent the transitional stage galaxies in the merger-driven galaxy evolution scenario is to investigate their $\lambda_{\rm Edd}$ values. In the scenario, dust-obscured quasars are expected to have higher $\lambda_{\rm Edd}$ values than unobscured quasars. However, determining $\lambda_{\rm Edd}$ values of dust-obscured quasars is a challenge task. Because, traditional $L_{\rm bol}$ and $M_{\rm BH}$ estimators (e.g., Richards et al. 2006a; Vestergaard & Peterson 2006; Shen et al. 2011) are based on UV or optical luminosity, and they are easily affected by dust extinction. In order to overcome this limitation of the UV- or optical-based estimators, several infrared (IR)-based estimators have been derived (e.g., Kim et al. 2010, 2015b, 2022, 2023). Using the IR-based estimators, several studies (e.g., Kim et al. 2015a, 2024a) showed that dust-obscured quasars have significantly higher $\lambda_{\rm Edd}$ values compared to unobscured quasars. However, even with the IR-based estimators, the studies of $\lambda_{\rm Edd}$ values of dust-obscured quasars face limitations due to (i) the limited sample sizes (e.g., $\lesssim$15; Urrutia et al. 2012; Kim et al. 2015a); (ii) the samples in limited and low redshift ranges (e.g., $z \sim 0.3, 0.7$, and $\lesssim$1; Kim et al. 2015a, 2018, 2024a).

Moreover, the merger-driven galaxy evolution scenario has not been tested at $z \sim 2$, a period which both star-formation and black hole accretion activities peak in the Universe (e.g., Madau et al. 1998; Richards et al. 2006a; Ross et al. 2013). At this redshift, although dust-obscured quasars have not yet been fully discovered due to various reasons (e.g., Glikman et al. 2012), they are believed to significantly affect studies on SMBH accretion efficiency (Yu & Tremaine 2002) and quasar luminosity function (Kim et al. 2024b). Therefore, expanding the studies on the intrinsic properties and formation mechanisms of dust-obscured quasars to $z \sim 2$ is important not only for testing the merger-driven galaxy evolution scenario but also for understanding the co-evolution of BHs and their host galaxies.

Recently, Ishikawa et al. (2023) discovered new dust-obscured quasars at $z \sim 2$ through IR spectroscopic observations. In this paper, we measure their $\lambda_{\rm Edd}$ values using recently established $L_{\rm MIR}$-based $L_{\rm bol}$ and $M_{\rm BH}$ estimators (Kim et al. 2023) that are highly resistant to dust extinction, and we compare them to unobscured quasars at the same redshift selected from the SDSS Data Release 14 (DR14) quasars (Pâris et al. 2018). Throughout this work, we use a standard ΛCDM model of $H_0 = 70\ {\rm km\,s^{-1}}$ Mpc^{-1}, $\Omega_m = 0.3$, and $\Omega_\Lambda = 0.7$. This model has been supported by several observational studies in the past decades (e.g. Im et al. 1997; Planck Collaboration et al. 2016).

2. Sample

Our sample is chosen from 23 dust-obscured quasars at $z \sim 2$ confirmed by Ishikawa et al. (2023). Ishikawa et al. (2023) selected dust-obscure quasar candidates using Wide-field Infrared Survey Explorer (WISE; Wright et al. 2010) and SDSS Stripe 82 (Jiang et al. 2014) photometry. In that study, the used selection criteria are (i) $W4 \leq 8$ mag (Vega); and (ii) $r > 23$ mag (AB), and the criteria primarily select objects with redshift between 1 and 3. Among the candidates, Ishikawa et al. (2023) obtained near-infrared (NIR) spectra for 24 dust-obscured quasar candidates using *Gemini*/GNIRS, and they confirmed 23 candidates as dust-obscured quasars with redshifts ranging from 0.88 to 2.99. Moreover, they measured Hα full width half maximum (FWHM) values for 16 dust-obscured quasars.

From the 16 dust-obscured quasars, we choose our sample using conventions that are revised from those used in Kim et al. (2024a). First, the measured Hα FWHM is greater than 2000 ${\rm km\,s^{-1}}$. This FWHM criterion is for excluding narrow-line Seyfert 1 (NLS1) galaxies (e.g., FWHM $\lesssim 200\ {\rm km\,s^{-1}}$; Zhou et al. 2006), since NLS1 galaxies may have systematically different $\lambda_{\rm Edd}$ values (Boroson 2002). Second, the measured quasar fractions at 3.4 μm and 4.6 μm from the SED fitting are greater than 0.5. Additionally, to investigate the $\lambda_{\rm Edd}$ of dust-obscured quasars at $z \sim 2$, we select only those objects with redshift between 1.5 and 2.5.

Finally, we select 10 objects as dust-obscured quasars at $z \sim 2$, which are listed in Table 1. The selected dust-obscured quasars have wide ranges of $M_{\rm BH}$ ($10^{8.76}$–$10^{9.78}$ $M_\odot$), $L_{\rm bol}$ ($10^{46.65}$–$10^{47.26}$ ${\rm erg\,s^{-1}}$), and redshift (1.53–2.48), and Figure 1 shows their basic properties.

To compare the dust-obscured quasars with unobscured quasars, we select unobscured quasars from SDSS DR14 quasars (Pâris et al. 2018). The spectral properties of these SDSS quasars were measured (Rakshit et al. 2020) by performing the `PyQSOFit` code (Guo et al. 2019; Shen et al. 2019). To minimize sample bias, we apply the same selection criteria to the SDSS quasars as to the dust-obscured quasars, which are: (i) $1.53 < z < 2.48$; and (ii) FWHM $> 2000\ {\rm km\,s^{-1}}$. Here, as the SDSS quasars have optical spectra, the FWHM criterion is applied to FWHM$_{\rm Mg\,II}$, and these FWHM$_{\rm Mg\,II}$ values are similar to those of FWHM$_{\rm H\alpha}$ ($\log {\rm FWHM_{H\alpha}} = \log {\rm FWHM_{Mg\,II}} - 0.012$; Bisogni et al. 2017). Additionally, we select the SDSS quasars within the $W4$ magnitude rage of the dust-obscured quasars ($7.04 < W4 < 7.98$). Finally, we add another selection criterion based on the results of Kim et al. (2023), which showed that ∼15% of SDSS quasars are also affected by dust extinction. Hence, we select SDSS quasars with a power-law slope of less than -0.2, where dust-extinction is negligible (Kim et al. 2023).

Through these selection criteria, we choose 2554 SDSS quasars as unobscured quasars. The selected unobscured quasars have ranges of $M_{\rm BH}$ ($10^{8.26}$–$10^{10.59}$ $M_\odot$) and $L_{\rm bol}$ ($10^{45.12}$–$10^{47.74}$ ${\rm erg\,s^{-1}}$), and their basic properties are also shown in Figure 1.

3. SED Fitting

For the dust-obscured quasars, we measure $L_{\rm bol}$ and $M_{\rm BH}$ values with $L_{\rm MIR}$-based estimators (Kim et al. 2023). Kim et al. (2023) established the estimators based on monochromatic continuum luminosities, λL_λ, at 3.4 μm and 4.6 μm

Table 1. Properties of dust-obscured quasars

Object Name	Redshift†	FWHM$_{\rm H\alpha}$ (km s^{-1})	log ($L^*_{4.6}$) (erg s^{-1})	log ($L_{\rm bol}$) (erg s^{-1})	log ($M_{\rm BH}$) ($M_\odot$)	log ($\lambda_{\rm Edd}$)
J0024−0012	1.528	2355±193	46.13±0.04	46.85±0.09	8.76±0.14	−0.004±0.159
J0041−0029	2.090	2780±1700	46.20±0.06	46.92±0.10	8.94±0.38	−0.116±0.384
J0149+0052	1.850	2370±450	46.32±0.04	47.04±0.10	8.85±0.19	0.089±0.203
J0150+0056	1.700	3300±1000	45.92±0.05	46.65±0.09	8.96±0.25	−0.414±0.255
J0213+0024	1.805	6896±300	46.26±0.03	46.98±0.09	9.78±0.15	−0.899±0.170
J0221+0050	2.480	4400±370	46.47±0.04	47.19±0.10	9.48±0.16	−0.390±0.178
J2229+0022	1.930	2840±1190	46.54±0.04	47.26±0.10	9.12±0.30	0.038±0.305
J2258−0022	2.420	2210±400	46.36±0.07	47.08±0.11	8.81±0.19	0.170±0.212
J2259−0009	1.885	2350±115	46.34±0.04	47.06±0.10	8.86±0.13	0.106±0.156
J2334+0031	2.095	4350±200	46.28±0.05	47.00±0.10	9.38±0.14	−0.477±0.168

†$z_{\rm best}$ values in Ishikawa et al. (2023), *Extinction-corrected $L_{4.6}$ values.

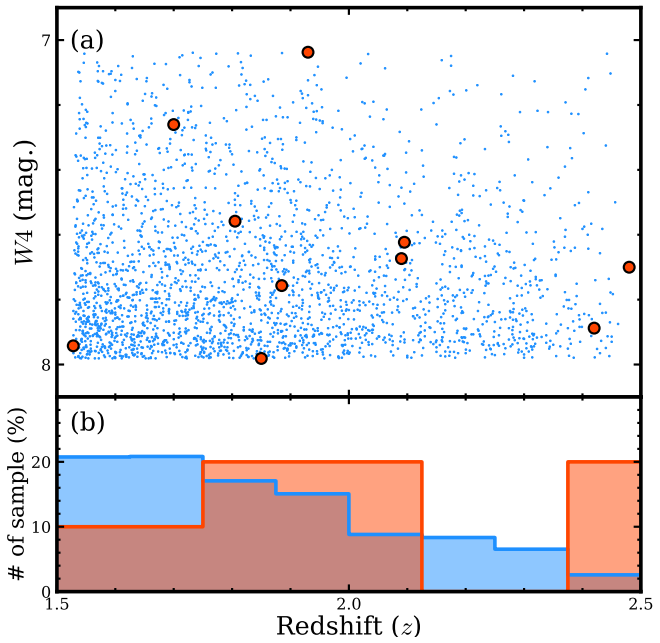

Figure 1. (a) Redshift versus $W4$-band magnitudes. Red circles and blue dots mean the dust-obscured quasars and unobscured quasars, respectively. (b) Redshifts of the two kinds of quasars. Red and blue histograms denote the dust-obscured quasars and the unobscured quasars, respectively.

(hereafter, $L_{3.4}$ and $L_{4.6}$, respectively) in the rest-frame, and these $L_{\rm MIR}$ values can be measured by performing SED fitting with their photometric data. Since the $L_{\rm MIR}$-based estimators are negligibly affected by dust extinction, they are ideal tools to measure the properties of dust-obscured quasars. Moreover, these $L_{\rm MIR}$ values are relatively free from their host galaxy contaminations (e.g., <20%; Kim et al. 2023). In contrast, contaminations from the host galaxies in the near-infrared (NIR) wavelength region is quite significant (e.g., ≳50%; Kim et al. 2023).

For the SED fitting, we use photometric data from SDSS Stripe 82 (Jiang et al. 2014), the UKIRT Infrared Deep Sky Survey (UKIDSS; Lawrence et al. 2007), and AllWISE (Cutri et al. 2021), after correcting for Galactic extinction (Schlafly & Finkbeiner 2011) based on an assumption of $R_V = 3.1$ (Weingartner & Draine 2001). While Kim et al. (2023) and Kim et al. (2024a) included Two Micron All-Sky Survey (2MASS; Skrutskie et al. 2006) data to cover the NIR wavelength region, this study opts for the UKIDSS data because our dust-obscured quasars are faint and poorly detected by the 2MASS survey.

Although SDSS Stripe 82 and UKIDSS data are deeper than SDSS and 2MASS data respectively, some of our dust-obscured quasars remain undetected due to their relatively high redshifts and significant dust extinction with $A_V \sim 4.8 \pm 2.8$ mag (Ishikawa et al. 2023). For the undetected filters, we apply upper limits during the SED fitting and adopt the χ^2 derivation method for the undetected filters (Sawicki 2012). The χ^2 method for the undetected filters has been widely used (e.g., Kim et al. 2019), and the χ^2 derivation is given by:

$$\chi^2_j = -2\ln\left[\sqrt{\frac{\pi}{2}}\sigma_j\left\{1+\mathbf{erf}\left(\frac{f_{{\rm lim},j}-f_{{\rm model},j}}{\sqrt{2}\sigma_j}\right)\right\}\right] \quad (1)$$

where $f_{{\rm lim},j}$ is the upper limit flux for filter j, $f_{{\rm model},j}$ is the model flux for filter j, and σ_j is the sensitivity in filter j.

The SED fitting is performed using a method similar to that of Kim et al. (2023, 2024a) and Kim et al. (2024b). The photometric data, $f(\lambda)$, of the dust-obscured quasars are fitted with an SED model composed of reddened spectra from a quasar $[Q(\lambda)]$, an elliptical galaxy $[E(\lambda)]$, a spiral galaxy $[S(\lambda)]$, and an irregular galaxy $[I(\lambda)]$. The SED model can be expressed as

$$f(\lambda) = C_1 Q(\lambda) + C_2 E(\lambda) + C_3 S(\lambda) + C_4 I(\lambda), \quad (2)$$

where C_1, C_2, C_3, and C_4 are the normalization constants of each component. The reddened spectrum $[X(\lambda)]$ can be derived from an intrinsic spectrum $[X_0(\lambda)]$ given an $E(B-V)$ value, as shown in the equation:

$$X(\lambda) = X_0(\lambda)\, 10^{-k(\lambda)E(B-V)/1.086}, \quad (3)$$

where $k(\lambda)$ is the reddening law (Fitzpatrick 1999), measured from Galactic extinction curve with $R_V = 3.1$ (Weingartner

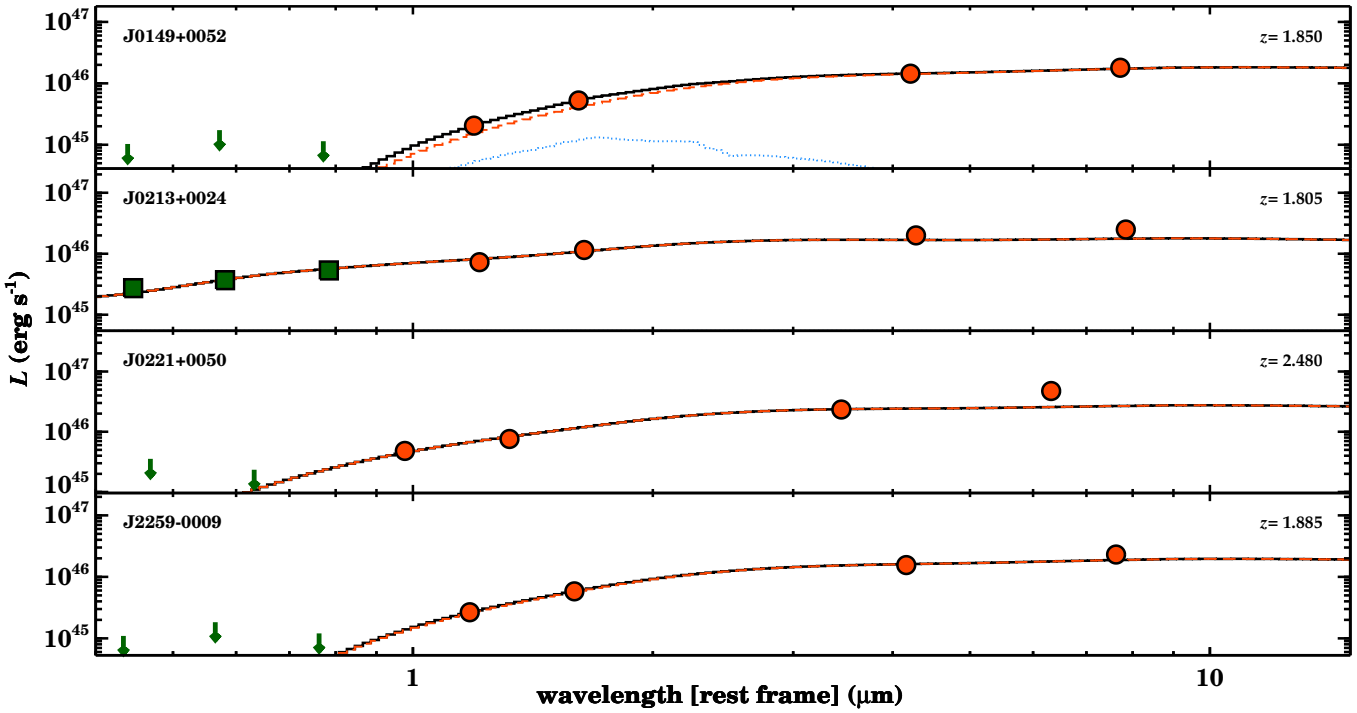

Figure 2. Photometric data and fitted SED models of four randomly selected dust-obscured quasars. Green squares and red circles denote the photometric data points of UKIDSS and WISE, respectively, while green arrows represent the limiting fluxes of UKIDSS for the undetected filters. Black solid lines mean the best-fit SED models, and red dashed and blue dotted lines are the reddened spectra of quasar and host galaxy, respectively.

& Draine 2001). For the intrinsic quasar spectrum, the quasar spectral template of Krawczyk et al. (2013) is adopted, while three types of galaxy spectral templates in Assef et al. (2010) are used for the intrinsic galaxy spectra. Note that there are several other quasar templates (e.g., Richards et al. 2006b; Assef et al. 2010). However, their SED shapes are similar to those of Krawczyk et al. (2013), and using the different templates does not significantly affect the measured $L_{\rm MIR}$ values (Kim et al. 2023).

During the SED fitting, we use an interactive data language (IDL) procedure, `MPFIT` (Markwardt 2009), to fit the photometric data, and Figure 2 shows examples of the best-fit SED model. Through the SED fitting, we obtain extinction-corrected $L_{3.4}$ and $L_{4.6}$ values of the dust-obscured quasars, and these $L_{4.6}$ values are summarized in Table 1.

The SED fitting also yields $E(B-V)$ values, and these $E(B-V)$ values can be precisely measured with optical-to-MIR photometric data. For the dust-obscured quasars, however, in cases where optical and/or NIR photometric data are undetected, this may lead to potentially inaccurate $E(B-V)$ estimates. Nevertheless, since the effects of extinction correction are negligible at 3.4 μm and 4.6 μm, these inaccuracies in the $E(B-V)$ measurements do not substantially affect the extinction-corrected $L_{4.6}$ values. For example, if a dust-obscured quasar with a color excess of $E(B-V) = 1$ mag is incorrectly measured as $E(B-V) = 2$ mag, then the extinction-corrected $L_{4.6}$ would be overestimated by only 0.05 dex.

4. Bolometric Luminosities and Black Hole Masses

In this section, we measure $L_{\rm bol}$ and $M_{\rm BH}$ values for both dust-obscured and the unobscured quasars. For the dust-obscured quasars, we use the $L_{\rm MIR}$-based estimators (Kim et al. 2023) for avoiding the effects of dust extinction. Although the $L_{\rm MIR}$-based estimators were originally established using unobscured quasars at $z \lesssim 0.5$, Kim et al. (2024a) showed that these estimators are still reliable up to a redshift of $z = 2.5$. Therefore, the $L_{\rm MIR}$-based estimators can be used for the dust-obscured quasars in this study. For the unobscured quasars, since dust extinction is not significant, we measure their $L_{\rm bol}$ and $M_{\rm BH}$ values using well-known continuum luminosity, λL_{λ}, at 3000 Å ($L3000$)-based estimators (Runnoe et al. 2012).

4.1. Bolometric Luminosities

To obtain bolometric luminosities of the dust-obscured quasars, we use the extinction-corrected $L_{4.6}$ values with the $L_{4.6}$-based $L_{\rm bol}$ estimator of Kim et al. (2023). The $L_{4.6}$-based $L_{\rm bol}$ estimator is

$$\log\left(\frac{L_{\rm bol}}{10^{44}\ {\rm erg\,s^{-1}}}\right) = (0.739 \pm 0.021) + (0.993 \pm 0.031)\ \log\left(\frac{L_{4.6}}{10^{44}\ {\rm erg\,s^{-1}}}\right), \quad (4)$$

and the measured $L_{\rm bol}$ values of the dust-obscured quasars are summarized in Table 1.

For the unobscured quasars, we use the $L3000$-based $L_{\rm bol}$ estimator (Runnoe et al. 2012). The $L3000$-based $L_{\rm bol}$ estimator is

$$\log\left(\frac{L_{\rm bol}}{10^{44}\,{\rm erg\,s^{-1}}}\right) = (0.53\pm1.27)+(0.97\pm0.03)\log\left(\frac{L3000}{10^{44}\,{\rm erg\,s^{-1}}}\right). \quad (5)$$

4.2. BH Masses

To measure BH masses of the dust-obscured quasars, we use the extinction-corrected $L_{4.6}$ values with the $L_{4.6}$-based $M_{\rm BH}$ estimator of Kim et al. (2023). Their $M_{\rm BH}$ values can be measured with $L_{4.6}$ and ${\rm FWHM_{H\alpha}}$ values, as

$$\log\left(\frac{M_{\rm BH}}{M_\odot}\right) = (6.97\pm0.06)+(0.48\pm0.02)\log\left(\frac{L_{4.6}}{10^{44}\,{\rm erg\,s^{-1}}}\right) + (2.06\pm0.06)\log\left(\frac{{\rm FWHM_{H\alpha}}}{1000\,{\rm km\,s^{-1}}}\right). \quad (6)$$

For the ${\rm FWHM_{H\alpha}}$ values, we adopt these values of the dust-obscured quasars from Ishikawa et al. (2023), which were measured by using *Gemini*/GNIRS spectroscopic observations. Note that the ${\rm FWHM_{H\alpha}}$ uncertainties of the dust-obscured quasars are ∼20%, which correspond to 0.16 dex and dominates the $M_{\rm BH}$ errors.

However, since the unobscured quasars have only optical spectral properties (Rakshit et al. 2020), we measure their $M_{\rm BH}$ values with $L3000$ and ${\rm FWHM_{Mg\,II}}$ values. To obtain a $M_{\rm BH}$ estimator with $L3000$ and ${\rm FWHM_{Mg\,II}}$ for the unobscured quasars, we use two relationships: between $L_{4.6}$ and $L3000$, and between ${\rm FWHM_{H\alpha}}$ and ${\rm FWHM_{Mg\,II}}$. The relationship between $L_{4.6}$ and $L3000$ can be obtained by combining Equations (5) and (6), and we adopt the relationship between ${\rm FWHM_{H\alpha}}$ and ${\rm FWHM_{Mg\,II}}$ from Bisogni et al. (2017). Recently, Bisogni et al. (2017) obtained optical to NIR spectra simultaneously using the X-shooter spectrograph (Vernet et al. 2011) on the Very Large Telescope (VLT) for quasars at $z\sim2.2$, and measured their ${\rm FWHM_{H\alpha}}$ and ${\rm FWHM_{Mg\,II}}$ values. The found relationship is

$$\log\left(\frac{{\rm FWHM_{H\alpha}}}{1000\,{\rm km\,s^{-1}}}\right) = \log\left(\frac{{\rm FWHM_{Mg\,II}}}{1000\,{\rm km\,s^{-1}}}\right)-(0.012\pm0.048). \quad (7)$$

By combining these two relationships into Equation (7), we derived the new BH mass estimator based on $L3000$ and ${\rm FWHM_{Mg\,II}}$, and the derived $M_{\rm BH}$ estimator is

$$\log\left(\frac{M_{\rm BH}}{M_\odot}\right) = (7.05\pm0.62)+(0.47\pm0.03)\log\left(\frac{L3000}{10^{44}\,{\rm erg\,s^{-1}}}\right) + (2.06\pm0.06)\log\left(\frac{{\rm FWHM_{Mg\,II}}}{1000\,{\rm km\,s^{-1}}}\right). \quad (8)$$

Using the $M_{\rm BH}$ estimator, we measure BH masses of the unobscured quasars. Note that the newly derived $M_{\rm BH}$ estimator is similar to the well-known $M_{\rm BH}$ estimator of Vestergaard & Osmer (2009) that is $M_{\rm BH}/M_\odot = 10^{6.86}\times\left[L3000/\left(10^{44}\,{\rm erg\,s^{-1}}\right)\right]^{0.5}\left[{\rm FWHM_{Mg\,II}}/\left(1000\,{\rm km\,s^{-1}}\right)\right]^2$.

5. Eddington Ratios

We measure $\lambda_{\rm Edd}$ ($L_{\rm bol}/L_{\rm Edd}$, where $L_{\rm Edd}$ is Eddington luminosity) values of the dust-obscured and the unobscured quasars with the $L_{\rm bol}$ and $M_{\rm BH}$ values measured in Section 4. The measured $\lambda_{\rm Edd}$ values of the dust-obscured quasars are summarized in Table 1. Uncertainties in the logarithmic values of $\lambda_{\rm Edd}$ values are in the range of 0.16 to 0.38, and the uncertainties are dominated by the errors in the $M_{\rm BH}$ measurements.

We compare the $\lambda_{\rm Edd}$ values of the dust-obscured to those of the unobscured quasars, as shown in Figures 3 and 4. The median $\log(\lambda_{\rm Edd})$ of the dust-obscured quasars is -0.06 ± 0.10, significantly higher than that of the unobscured quasars, which is -0.86 ± 0.01. To quantify the significance of difference in these $\lambda_{\rm Edd}$ distributions, we perform a Kolmogorov-Smirnov (K-S) test using the `SciPy` package. For the K-S statistics, a maximum deviation, D, between the cumulative distributions is found to be 0.79, and a probability, p, of the null hypothesis is found to be only 4.62×10^{-7}. These K-S statistics confirm that the $\lambda_{\rm Edd}$ values of the dust-obscured quasars are significantly higher than those of the unobscured quasars. This result is consistent with the previous studies (Kim et al. 2015a, 2024a; Urrutia et al. 2012), which support the merger-driven galaxy evolution scenario where dust-obscured quasars are in the intermediate stage galaxies between ULIRGs and unobscured quasars.

Moreover, we compare the $\lambda_{\rm Edd}$ values of the dust-obscured and the unobscured quasars across redshift from 1.5 to 2.5. For this comparison, we divide both types of quasars into four redshift bins: $1.5\le z<1.75$, $1.75\le z<2$, $2\le z<2.25$, and $2.25\le z<2.5$, and measure the $\lambda_{\rm Edd}$ values in each redshift bin. The $\log(\lambda_{\rm Edd})$ values of the dust-obscured quasars range from -0.30 to -0.11, but these values do not show any substantial changes with redshift. However, the $\log(\lambda_{\rm Edd})$ values of the unobscured quasars slightly increase from -0.94 to -0.70 as redshift increases, which is a trend that could arise from selection effects or cosmological evolution. The comparison is shown in Figure 5, where we find that the $\lambda_{\rm Edd}$ values of the dust-obscured quasars are significantly higher than those of the unobscured quasars within the redshift range of 1.5 and 2.5.

6. Dicussion

6.1. A Comparison of Bolometric Luminosities of Dust-Obscured Quasars Using Different Measurement Methods

The $L_{\rm bol}$ values of the dust-obscured quasars were also measured in Ishikawa et al. (2023) using a different measurement method. They derived the $L_{\rm bol}$ values based on the monochromatic luminosity at 3.5 μm (hereafter, $L_{3.5}$) by applying an IR

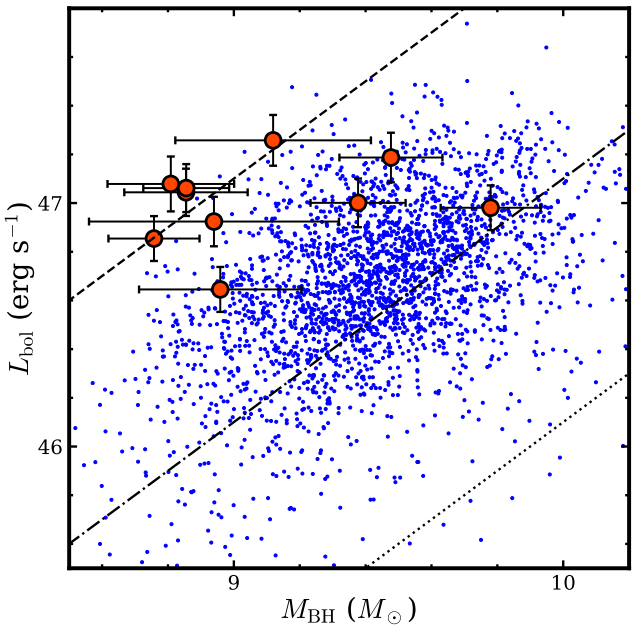

Figure 3. $L_{\rm bol}$ vs. $M_{\rm BH}$ of dust-obscured and unobscured quasars. The dust-obscured and the unobscured quasars are marked with red open circles and blue dots, respectively, and the dashed, dash-dotted, and dotted lines represent $\lambda_{\rm Edd}$ values of 1.0, 0.1, and 0.01, respectively.

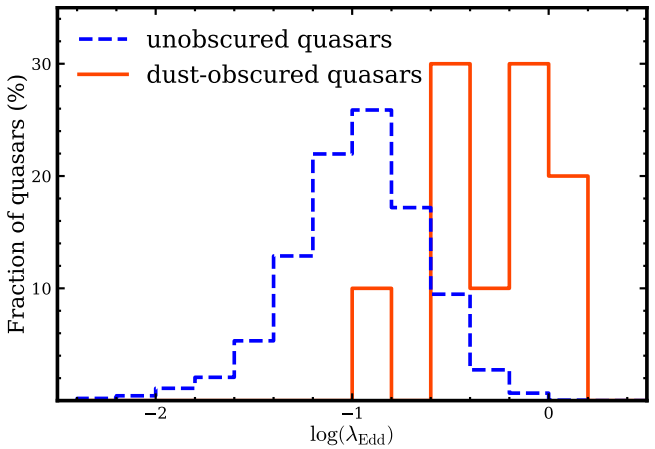

Figure 4. Distributions of $\log(\lambda_{\rm Edd})$ values for dust-obscured and unobscured quasars. Red solid histogram represents the dust-obscured quasars, and blue dashed histogram mean the unobscured quasars.

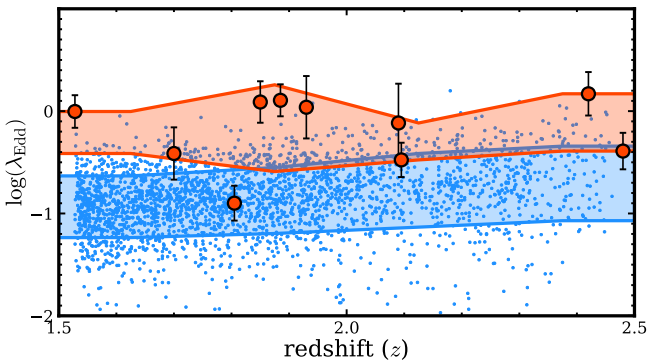

Figure 5. Redshifts versus $\log(\lambda_{\rm Edd})$ values for dust-obscured and unobscured quasars. Red open circles and blue dots represent the dust-obscured and the unobscured quasars, respectively. Red and blue polygons indicate the mean $\log\lambda_{\rm Edd}$ values and their standard deviations at each redshift bin for the dust-obscured and the unobscured quasars, respectively.

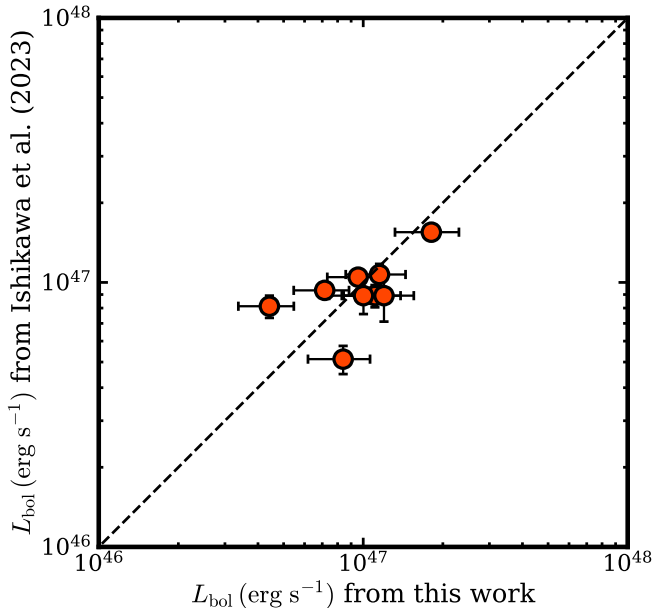

Figure 6. Comparison of bolometric luminosities of dust-obscured quasars from this work and Ishikawa et al. (2023). Dashed line means the case where the $L_{\rm bol}$ values are identical.

bolometric correction factor of 8 (Hamann et al. 2017; Perrotta et al. 2019). The $L_{3.5}$ values were determined by extrapolating L_5 (monochromatic luminosity at 5 μm) assuming a power-law SED shape. Note that these $L_{\rm bol}$ uncertainties were measured to be relatively small because they do not include the uncertainty of the bolometric correction factor (at least a factor of 2; Hamann et al. 2017).

We compare the $L_{\rm bol}$ values of the dust-obscured quasars from this work to those from Ishikawa et al. (2023), and we present this comparison in Figure 6. Note that we excluded J0221+0050 in this analysis, because the $L_{\rm bol}$ value of this object in Table 2 of Ishikawa et al. (2023) is likely to be in error (listed a value too small) after examining their Figure 5 and comparing $L_{\rm bol}$ value of this object to J2329+0022, a quasar with very similar properties to J0221+0050. We find a reasonable agreement between the two $L_{\rm bol}$ measurements, and the Pearson correlation coefficient is 0.57. Although the measured Pearson correlation coefficient is relatively low, there are several possible reasons for this. First, when Ishikawa et al. (2023) measured the $L_{\rm bol}$ values, they assumed a power-law of $L_\lambda \propto \lambda^\alpha$, where α is 1.05 ± 0.6 at 5 μm. This diversity of α can introduce an uncertainty of $\sim$0.10 dex in $L_{\rm bol}$, resulting in inaccurate $L_{\rm bol}$ measurements. Second, in our SED fit, the SDSS, UKIDSS, and WISE photometric data were not measured simultaneously, which could have led to an inaccurate $L_{\rm bol}$ because quasar variability causes the photometric SED shape to differ from the templates.

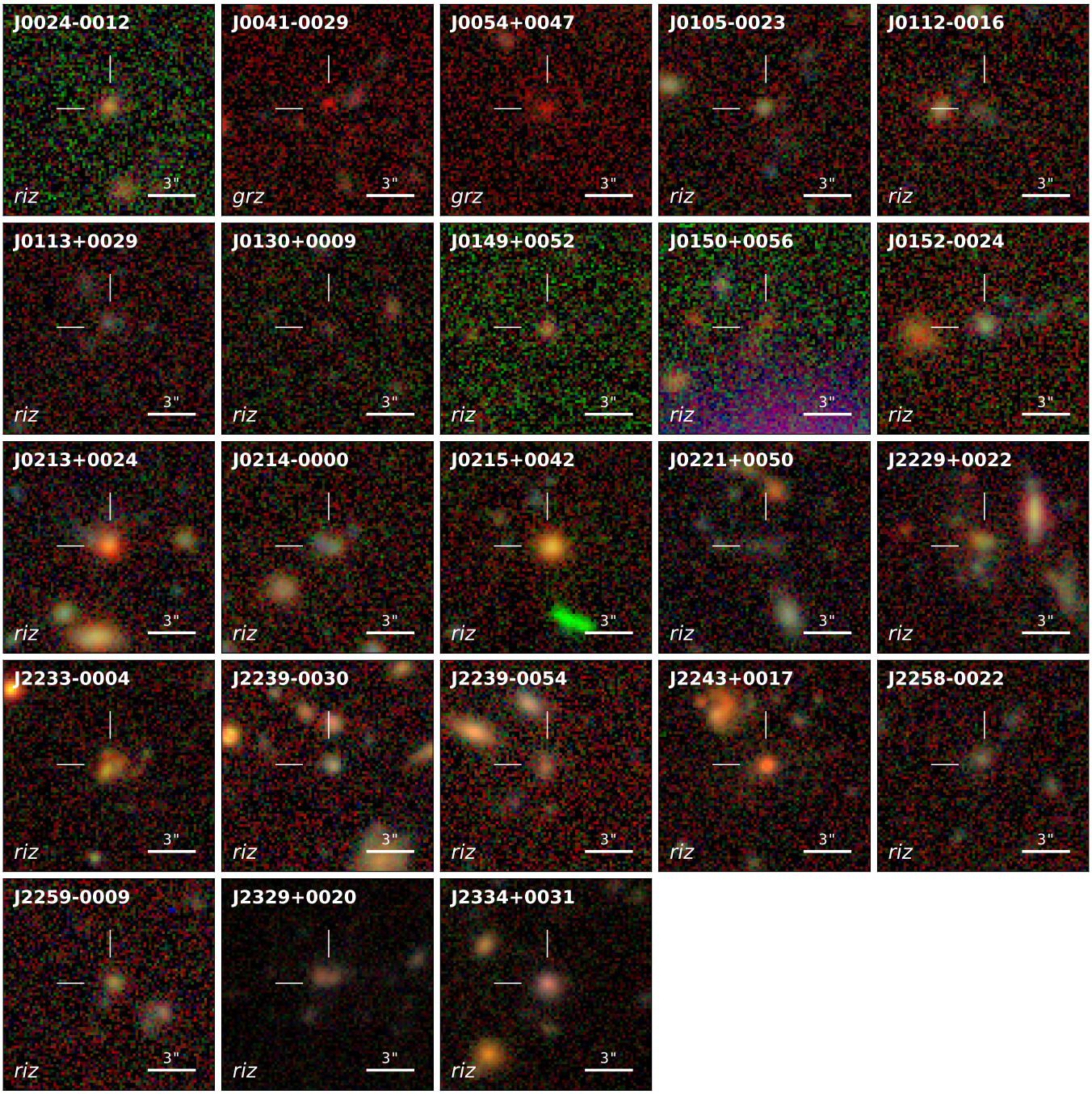

Figure 7. HSC color (*riz* or *grz* filters) images of 23 dust-obscured quasars at $z \sim 2$, and these objects are marked in white reticles. Bottom white bars indicate 3″, which correspond to ∼25 kpc.

If we adopt the $L_{\rm bol}$ values from Ishikawa et al. (2023), the median $\log(\lambda_{\rm Edd})$ value of the dust-obscured quasars slightly increases to -0.03 ± 0.10, after excluding J0221+0050. Thus, regardless of whether we use the $L_{\rm bol}$ values from this work or those from Ishikawa et al. (2023), the result consistently shows that the $\lambda_{\rm Edd}$ values of the dust-obscured quasars are significantly higher than those of the unobscured quasars.

6.2. Investigations on Host Galaxies of Dust-Obscured Quasars Using HSC-SSP Data: Opportunities and Prospects

In the merger-driven galaxy evolution scenario, dust-obscured quasars are expected to have merging host galaxies. Urrutia et al. (2008) investigated 13 dust-obscured quasars at $z < 1$ using the Hubble Space Telescope (HST) images and confirmed that ∼85% of these objects exhibit clear evidence of merging features. Furthermore, Glikman et al. (2015) observed 11 dust-obscured quasars at $z \sim 2$ with the HST, and found that ∼80% of these objects also have actively merging hosts.

Most studies on the host galaxies of dust-obscured quasars

have used the HST data. The high spatial resolution data provided from the HST have allowed for successful investigations, but previous studies (e.g., Urrutia et al. 2008; Glikman et al. 2015) were limited to small sample size ($\leq$15) due to scarcity of the HST data. Consequently, obtaining statistically robust results on whether dust-obscured quasars typically have merging host galaxies has been challenging.

Recently, Hyper Suprime-Cam Subaru Strategic Program (HSC-SSP; Aihara et al. 2022) data were released. The HSC-SSP covers ∼670 $\deg^2$ in the *grizy* bands, with the seeing ranging from 0.″6 to 0.″8. Considering this coverage and seeing of the HSC-SSP data, it is expected that a statistically sufficient number of dust-obscured quasars' host galaxies can be investigated.

In this subsection, we explore the feasibility of studying the host galaxies of dust-obscured quasars using the HSC-SSP data. We check the HSC-SSP data for 23 dust-obscured quasars at $z \sim 2$ listed in Ishikawa et al. (2023). Among these objects, two objects (J2329+0020 and J2334+0031) are covered by the HSC-SSP Deep survey, while the rest of them are included in the HSC-SSP Wide survey area. Using the HSC-SSP data, we find tentative evidence of merging features, such as disturbed appearance, multiple nuclei, or close companions within tens of kpc, for some of these dust-obscured quasars (e.g., J2229+0022, J2233−0004, and J2329+0020), as shown in Figure 7. However, most objects appear too faint or too small to reliably classify if they are merging systems or not.

It is difficult to find clear merging features with the current HSC-SSP data, and even the tentative merging features are not as easily detectable as those in the previous studies with the HST (e.g., ∼80%; Urrutia et al. 2008; Glikman et al. 2015). However, our findings suggest that the HSC-SSP data allow us (i) to find the tentative evidence for merging features in the host galaxies of some dust-obscured quasars at $z \sim 2$; (ii) to easily find merging features in the host galaxies of dust-obscured quasars at low redshifts considering the reduced cosmological surface brightness dimming.

With upcoming surveys, such as Spectro-Photometer for the History of the Universe, Epoch of Reionization, and Ices Explorer (SPHEREx; Doré et al. 2014) and Legacy Survey of Space and Time (LSST; Ivezić et al. 2019), hundreds of thousands of dust-obscured quasars at low redshifts are expected to be discovered or revealed to be obscured by dust. This expectation is based on previous studies (e.g., Comastri et al. 2001; Polletta et al. 2008) that suggest dust-obscured quasars occupy ∼50% of the entire quasar population. Therefore, these upcoming surveys will promote more extensive investigations into the host galaxies of dust-obscured quasars with the HSC-SSP data.

7. Conclusion

We measured $L_{\rm bol}$ and $M_{\rm BH}$ values of 10 dust-obscured quasars at $z \sim 2$ using $L_{\rm MIR}$-based estimators (Kim et al. 2023). The $L_{\rm MIR}$-based estimators are highly resistant to dust extinction, and these $L_{\rm MIR}$ values were measured by performing the SED fitting with the photometric data.

Using the measured $L_{\rm bol}$ and $M_{\rm BH}$ values, we compare the $\lambda_{\rm Edd}$ values of the dust-obscured quasars to those of unobscured quasars at the same redshift selected from the SDSS DR14 quasars (Pâris et al. 2018). We found that the $\lambda_{\rm Edd}$ values of the dust-obscured quasars, -0.06 ± 0.10, are significantly higher than those of the unobscured quasars, -0.86 ± 0.01. Moreover, this result is consistent across the redshift range from 1.5 to 2.5.

Previous observational studies showed that dust-obscured quasars have (i) high $\lambda_{\rm Edd}$ values across different redshifts (Kim et al. 2015a, 2023; Urrutia et al. 2012); (ii) dusty red colors (Kim & Im 2018); (iii) merging features in their host galaxies (Urrutia et al. 2008; Glikman et al. 2015); and (iv) merging SMBH system candidates (Kim et al. 2020). When considering both our results and these previous studies, these findings strongly support the merger-driven galaxy evolution scenario, suggesting that dust-obscured quasars are the intermediate population between merger-driven star-forming galaxies, ULIRGs, and unobscured quasars.

Acknowledgments

We thank the anonymous referee for the useful comments. This work was supported by the National Research Foundation of Korea (NRF) grant funded by the Korea government (MSIT) (Nos. 2021R1C1C1013580, 2022R1A4A3031306, 2020R1A2C3011091, 2021M3F7A1084525, 2022R1A6A-3A01085930, and 2021R1C1C2091550).

References

Aihara, H., AlSayyad, Y., Ando, M., et al. 2022, PASJ, 74, 247
Assef, R. J., Kochanek, C. S., Brodwin, M., et al. 2010, ApJ, 713, 970
Becker, R. H., White, R. L., Gregg, M. D., et al. 2001, ApJS, 135, 227
Bisogni, S., di Serego Alighieri, S., Goldoni, P., et al. 2017, A&A, 603, A1
Boroson, T. A. 2002, ApJ, 565, 78
Comastri, A., Fiore, F., Vignali, C., et al. 2001, MNRAS, 327, 781
Croom, S. M., Smith, R. J., Boyle, B. J., et al. 2004, MNRAS, 349, 1397
Cutri, R. M., Wright, E. L., Conrow, T., et al. 2021, VizieR Online Data Catalog, II/328
Doré, O., Bock, J., Ashby, M., et al. 2014, arXiv e-prints, arXiv:1412.4872
Fitzpatrick, E. L. 1999, PASP, 111, 63
Georgantopoulos, I., Pouliasis, E., Mountrichas, G., et al. 2023, A&A, 673, A67
Glikman, E., Simmons, B., Mailly, M., et al. 2015, ApJ, 806, 218
Glikman, E., Urrutia, T., Lacy, M., et al. 2012, ApJ, 757, 51
Guo, H., Liu, X., Shen, Y., et al. 2019, MNRAS, 482, 3288
Hamann, F., Zakamska, N. L., Ross, N., et al. 2017, MNRAS, 464, 3431
Hopkins, P. F., Hernquist, L., Cox, T. J., & Kereš, D. 2008, ApJS, 175, 356
Im, M., Griffiths, R. E., & Ratnatunga, K. U. 1997, ApJ, 475, 457

Ishikawa, Y., Wang, B., Zakamska, N. L., et al. 2023, MNRAS, 522, 350
Ivezić, Ž., Kahn, S. M., Tyson, J. A., et al. 2019, ApJ, 873, 111
Jiang, L., Fan, X., Bian, F., et al. 2014, ApJS, 213, 12
Kim, D., & Im, M. 2018, A&A, 610, A31
Kim, D., Im, M., Glikman, E., Woo, J.-H., & Urrutia, T. 2015a, ApJ, 812, 66
Kim, D., Im, M., & Kim, M. 2010, ApJ, 724, 386
Kim, D., Im, M., Kim, M., & Ho, L. C. 2020, ApJ, 894, 126
Kim, D., Im, M., Kim, M., et al. 2023, ApJ, 954, 156
Kim, D., Lee, D., & Im, M. 2022, MNRAS, 509, 1147
Kim, D., Im, M., Kim, J. H., et al. 2015b, ApJS, 216, 17
Kim, D., Im, M., Canalizo, G., et al. 2018, ApJS, 238, 37
Kim, D., Kim, Y., Im, M., et al. 2024a, A&A, submitted
Kim, Y., Im, M., Jeon, Y., et al. 2019, ApJ, 870, 86
Kim, Y., Kim, D., Im, M., et al. 2024b, ApJ, submitted
Krawczyk, C. M., Richards, G. T., Mehta, S. S., et al. 2013, ApJS, 206, 4
Lawrence, A., Warren, S. J., Almaini, O., et al. 2007, MNRAS, 379, 1599
Madau, P., Pozzetti, L., & Dickinson, M. 1998, ApJ, 498, 106
Markwardt, C. B. 2009, in ASP Conf. Ser., Vol. 411, Astronomical Data Analysis Software and Systems XVIII, ed. D. A. Bohlender, D. Durand, & P. Dowler, 251
Menci, N., Cavaliere, A., Fontana, A., et al. 2004, ApJ, 604, 12
Pâris, I., Petitjean, P., Aubourg, É., et al. 2018, A&A, 613, A51
Perrotta, S., Hamann, F., Zakamska, N. L., et al. 2019, MNRAS, 488, 4126
Planck Collaboration, Ade, P. A. R., Aghanim, N., et al. 2016, A&A, 594, A13
Polletta, M., Weedman, D., Hönig, S., et al. 2008, ApJ, 675, 960
Puchnarewicz, E. M., & Mason, K. O. 1998, MNRAS, 293, 243
Rakshit, S., Stalin, C. S., & Kotilainen, J. 2020, ApJS, 249, 17
Richards, G. T., Strauss, M. A., Fan, X., et al. 2006a, AJ, 131, 2766
Richards, G. T., Lacy, M., Storrie-Lombardi, L. J., et al. 2006b, ApJS, 166, 470
Rose, M., Tadhunter, C. N., Holt, J., & Rodríguez Zaurín, J. 2013, MNRAS, 432, 2150
Ross, N. P., McGreer, I. D., White, M., et al. 2013, ApJ, 773, 14
Runnoe, J. C., Brotherton, M. S., & Shang, Z. 2012, MNRAS, 422, 478
Sanders, D. B., Soifer, B. T., Elias, J. H., et al. 1988, ApJ, 325, 74
Sawicki, M. 2012, PASP, 124, 1208
Schlafly, E. F., & Finkbeiner, D. P. 2011, ApJ, 737, 103
Schneider, D. P., Hall, P. B., Richards, G. T., et al. 2005, AJ, 130, 367
Shen, Y., Richards, G. T., Strauss, M. A., et al. 2011, ApJS, 194, 45
Shen, Y., Hall, P. B., Horne, K., et al. 2019, ApJS, 241, 34
Skrutskie, M. F., Cutri, R. M., Stiening, R., et al. 2006, AJ, 131, 1163
Urrutia, T., Lacy, M., & Becker, R. H. 2008, ApJ, 674, 80
Urrutia, T., Lacy, M., Spoon, H., et al. 2012, ApJ, 757, 125
Vernet, J., Dekker, H., D'Odorico, S., et al. 2011, A&A, 536, A105
Véron-Cetty, M. P., & Véron, P. 2006, A&A, 455, 773
Vestergaard, M., & Osmer, P. S. 2009, ApJ, 699, 800
Vestergaard, M., & Peterson, B. M. 2006, ApJ, 641, 689
Weingartner, J. C., & Draine, B. T. 2001, ApJ, 548, 296
Whiting, M. T., Webster, R. L., & Francis, P. J. 2001, MNRAS, 323, 718
Wilkes, B. J., Schmidt, G. D., Cutri, R. M., et al. 2002, ApJ, 564, L65
Wright, E. L., Eisenhardt, P. R. M., Mainzer, A. K., et al. 2010, AJ, 140, 1868
York, D. G., Adelman, J., Anderson, John E., J., et al. 2000, AJ, 120, 1579
Yu, Q., & Tremaine, S. 2002, MNRAS, 335, 965
Zhou, H., Wang, T., Yuan, W., et al. 2006, ApJS, 166, 128